



# A finite element analysis of pneumatic-tire/sand interactions during off-road vehicle travel

M. Grujicic, H. Marvi, G. Arakere and I. Haque  
*Department of Mechanical Engineering,  
International Center for Automotive Research CU-ICAR,  
Clemson University, Clemson, South Carolina, USA*

## Abstract

**Purpose** – The purpose of this paper is to carry out a series of transient, non-linear dynamics finite element analyses in order to investigate the interactions between a stereotypical pneumatic tire and sand during off-road vehicle travel.

**Design/methodology/approach** – The interactions were considered under different combined conditions of the longitudinal and lateral slip as encountered during “brake-and-turn” and “drive-and-turn” vehicle maneuvers. Different components of the pneumatic tire were modeled using elastic, hyper- and visco-elastic material models (with rebar reinforcements), while sand was modeled using the CU-ARL sand models developed by Grujicic *et al.* The analyses were used to obtain functional relations between the wheel vertical load, wheel sinkage, tire deflection, (gross) traction, motion resistance and the (net) drawbar pull. These relations were next combined with Pacejka magic formula for a pneumatic tire/non-deformable road interaction to construct a tire/sand interaction model suitable for use in multi-body dynamics analysis of the off-road vehicle performance.

**Findings** – To rationalize the observed traction and motion resistance relations, a close examination of the distribution of the normal and shear contact stresses within the tire/sand contact patch is carried out and the results were found to be consistent with the experimental counter parts.

**Originality/value** – The paper offers insights into the interactions between a stereotypical pneumatic tire and sand during off-road vehicle travel.

**Keywords** Finite element analysis, Road vehicles

**Paper type** Research paper

## 1. Introduction

It is well-established that off-road vehicle performance, such as vehicle mobility, stability, maneuverability, etc. is generally affected and controlled by the pneumatic tire-off-road terrain interactions. However, due to non-linear nature of the mechanical response of materials within the tire and deformable terrain (sand, in the present work), non-linearity of tire/sand contact mechanics and variety of tire/sand operating conditions (i.e. combination of wheel vertical load, longitudinal slip and lateral slip), tire/sand contact forces are difficult to quantify (both experimentally and computationally). While it is relatively straightforward to measure experimentally the net drawbar pull force as the reaction force at the wheel hub, the gross-traction and motion resistance contributions to this force are difficult to separate/quantify.

The material presented in this paper is based on the work supported by a research contract with the Automotive Research Center at the University of Michigan and TARDEC. The authors are indebted to Professor Georges Fadel for the support and a continuing interest in the present work.



---

Consequently, direct measurements of tire/sand interactions while providing reliable data for the tire/sandy-road pair in question subjected to a given set of operating conditions provide limited opportunities for estimating the interaction forces, under other conditions and for other tire/sand combinations. Since the finite element analysis of the tire/sand interaction enables computation of the normal and shear stresses over the tire/sand contact patch and the integration of these stresses leads to the quantification of the interaction forces, it can overcome some of the aforementioned limitations of the experimental approach. This was clearly shown in the recent work of Lee and Kiu (2007) who carried out a comprehensive finite element-based investigation of the interactions between a pneumatic tire and fresh snow. Hence, the main objective of the present work is to extend the work of Lee and Kiu (2007) to the case of tire/sand interactions.

While both snow and sand are deformable terrain porous materials and are frequently modeled using similar material models (Shoop, 2001), they are essentially quite different. Among the key differences between snow and sand, the following ones are frequently cited:

- While compaction of snow under pressure involves considerable amounts of inelastic deformation of the snow flakes, plastic compaction of sand primarily involves inter-particle sliding and (under very high pressure and/or loading rates) sand-particle fragmentation.
- While snow tends to undergo a natural sintering process known as “metamorphism” (Arons and Colbeck, 1995) which greatly enhances cohesive strength of this material, dry sand is typically considered as a “cohesion-less” material.
- The extent of plastic compaction in snow (ca. 300-400 percent) is significantly higher than those in sand (ca. 40-60 percent), etc.

Owing to the aforementioned differences in the mechanical response of snow and sand, one could expect that important differences in the distributions of normal and shear stresses may exist within the tire/snow and the tire/sand contact patches. Thus, to better understand the nature of the gross traction and motion resistance forces and their dependence on the loading/driving conditions in the case of tire/sand interactions, a comprehensive finite element investigation of this problem (similar to that of Lee and Kiu, 2007) needs to be conducted. This was done in the present work.

Vehicle performance on unpaved surfaces is important to the military as well as to agriculture, forestry, mining and construction industries. The primary issues are related to the prediction of vehicle mobility (e.g. traction, draw-bar pull, etc.) and to the deformation/degradation of terrain due to vehicle passage. The central problem associated with the off-road vehicle performance and terrain changes is the interaction between a deformable tire and deformable unpaved road (i.e. sand/soil). Early efforts in understanding the tire/sand interactions can be traced to Bekker (1956, 1960, 1969) at the University of Michigan and the US Army Land Locomotion Laboratory. A good overview of the research done in this area from the early 1960s to the late 1980s can be found in two seminal books, one by Yong *et al.* (1984) and the other by Wong (1989). Over the last 25 years, there have been numerous investigations dealing with numerical modeling and simulations of tire/sand interactions. An excellent summary of these investigations can be found in Shoop (2001).

The work of Shoop (2001) represents one of the most comprehensive recent computational/field test investigations of tire/sand interactions. The effect of normal load on sand sinkage and motion resistance coefficient was studied. However, the study did not include the effects of controlled longitudinal slip and lateral slip at different levels of the vertical load; no attempt was made to separate the traction and the motion resistance and no effort was taken to derive the appropriate tire/sand interaction model needed in multi-body dynamics analyses of the off-road vehicle performance. These aspects of the tire/sand interactions will be addressed computationally in the present work.

The organization of the paper is as follows: the finite element model for a prototypical pneumatic tire is presented in Section 2.1. A brief overview of the material models used to describe the mechanical response of various components of the tire and of the sand-based terrain is provided in Section 2.2. Detailed descriptions of the tire and sand computational domains and of the finite element procedure employed to study tire/sand interactions during the off-road vehicle travel are given in Section 2.3. The main results obtained in the present work are presented and discussed in Section 3. A brief summary of the present work and the main conclusions are given in Section 4.

## 2. Model development and computational procedure

### 2.1 *Finite element model for pneumatic tire*

Before the problem of tire/sand interactions can be considered, a physically realistic tire model needs to be created and validated. Modern tires are structurally quite complex, consisting of layers of belts, plies and bead steel imbedded in rubber. Materials are often anisotropic, and rubber compounds vary throughout the tire structure. Models developed for tire design are extremely detailed, account for each material within the tire and enable computational engineering analyses of internal tire stresses, wear and vibrational response. However, since in the present work, only deformation of the tire regions in contact with sand and the tire's ability to roll over a deformable surface is of concern, a simpler model can be employed. This would provide for better computational efficiency without significant loss in essential physics of the tire/sand interactions. Toward that end, a simpler treaded tire model, described below, is developed and tested in the present work.

The tire considered in the present work (the Goodyear Wrangler HT 235/75 R15) is a modern radial tire, which is composed of numerous components. Each of these components contributes to the structural behavior of the tire and is considered either individually or en masse when creating deformable tire model. The tire direction convention used here is based on the SAE (1992) standard definitions for vehicle dynamics. That is, relative to the straight-ahead (pure) rolling condition of the tire, the tire's longitudinal axis is in the direction of travel and the lateral or transverse direction is perpendicular to travel and in the horizontal plane. The Goodyear Wrangler HT tire was evaluated in Shoop (2001) for its deformation characteristics (i.e. the deflection and the contact area) on a rigid surface. Tire deflection at a given level of inflation pressure is a primary measure of the tire structural response to vertical load. Deflection is defined as the difference between the unloaded and loaded section height and is usually normalized by the unloaded section height and reported in percents. A thorough discussion of tire mechanics can be found in Clark (1981).

The geometry and internal make-up of the Goodyear Wrangler HT LT 235/H5 R15 tire investigated in the present work were determined by cutting and examining/testing different portions of the tire. A typical finite element mesh used in the present work is shown in Figure 1, in which different components of the tire (e.g. tread, carcass, sidewall, the bead and the wheel rim) are labeled.

The tread, carcass and sidewall are modeled using ca. 35,000 eight-node solid elements with reduced integration and hourglass stiffening. Belt plies with a  $30^\circ$  crown angle are represented using ca. 10,000 embedded surface elements with rebar reinforcements, while the sidewall plies are represented using ca. 10,000 embedded surface elements with rebar reinforcements. The orientation of the rebar elements in different sections of the tire is shown in Figure 1. The tire bead, the wheel rim and the lug nuts are all modeled as a single rigid body.

To validate the aforementioned tire model, few finite element analyses were carried out in which the tire was inflated to different pressure levels and subjected to different normal loads (at the wheel-rim center) against a non-deformable road. Since the computed results, (presented in Section 3.1), pertaining to the tire deflection, were found to compare well with their experimental counterparts obtained in Shoop *et al.* (2006); the tire model was deemed reasonable and used in the remainder of the work.

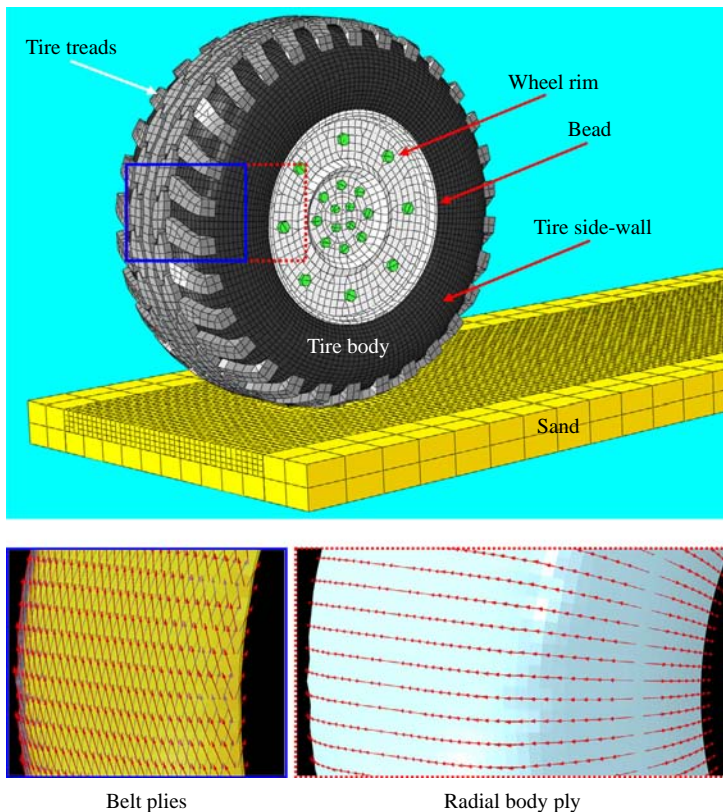


**Figure 1.** Computational meshed domains and rebar orientations used in the rolling analysis of a Goodyear Wrangler HT tire over deformable sand-based terrain

The sand-based terrain is modeled as a cuboidal region with the following dimensions:  $3,000 \times 1,050 \times 100$  mm in the length ( $x$ -direction), width ( $y$ -direction) and thickness ( $z$ -direction), respectively. The sand domain is meshed using ca. 25,000 eight-node solid elements with reduced integration and hourglass stiffening. Finer elements are used in the portion of the sand domain which is directly involved into the tire/sand interactions (Figure 1). It should be recalled that conventional choice of the co-ordinate system was made within which the tire moves in  $x$ -direction; its center of rotation is parallel with the  $y$ -direction, while  $z$ -direction is normal to the original top surface of the sand bed.

A parametric study was conducted to establish that sand bed is large enough and that the mesh size is fine enough that further changes in these quantities do not significantly affect the key computational results (e.g. magnitudes of the traction and motion-resistance forces, contact pressure and shear stress distributions, etc.). The results of these parametric studies are not shown for brevity.

### 2.2 Material models for tire components and sand

In this section, a brief overview is provided of the material models used to account for the mechanical response of various tire components and sand accompanying tire/sand interactions during off-road vehicle travel. Since many details regarding these models can be found either in the work of Lee and Kiu (2007) or in Grujicic *et al.* (2009a), only the key aspects of the material models will be covered.

**2.2.1 Tire material models.** Tread, carcass and sidewall are considered to be made of rubber whose mechanical response is assumed to be governed by its hyper- and visco-elastic behavior. The hyper-elastic portion of the rubber material model is represented using a strain-energy model as:

$$U = C_{10}(I_1 - 3) \quad (1)$$

where  $U$  is the strain energy and  $I_1$  is the first invariant of the (large deformation) deviatoric strain and  $C_{10}$  is the single hyper-elastic material parameter (set to 1.1 MPa Lee and Kiu, 2007).

The visco-elastic part of the rubber-material response is represented using one-term Prony series for the shear modulus. Within this model, the time-dependant shear modulus normalized by the instantaneous shear modulus,  $g(t) = G(t)/G_0$ , is defined as:

$$g(t) = 1 - g_1 \left( 1 - e^{-\frac{t}{\tau_1}} \right) \quad (2)$$

where  $g_1$  is the normalized shear-modulus relaxation parameter (0.3 (Lee and Kiu, 2007)), while  $\tau_1$  is the corresponding relaxation time (0.1 s (Lee and Kiu, 2007)).

The density of the rubber material is set to  $1,100 \text{ kg/m}^3$  (Lee and Kiu, 2007). Belts are considered to be made of an isotropic linear elastic material with a Young's modulus,  $E = 172.2 \text{ GPa}$ , the Poisson's ratio,  $\nu = 0.3$  and density  $\rho = 5,900 \text{ kg/m}^3$  (Lee and Kiu, 2007).

Carcass plies are also assumed to be made of an isotropic linear elastic material but with different properties:  $E = 9.876 \text{ Pa}$ ,  $\nu = 0.3$  and  $\rho = 1,500 \text{ kg/m}^3$  (Lee and Kiu, 2007).

**2.2.2 Sand material model.** As mentioned earlier, our recently developed model for sand, the CU-ARL sand model (Grujicic *et al.*, 2007), was used in the present work. This model was presented in great details in Grujicic *et al.* (2007) and, hence, only a brief

---

overview of it will be given in this section. Within the CU-ARL sand model, the relationships between the flow variables (pressure, mass-density, energy-density, temperature, etc.) are defined in terms of:

- an equation of state;
- a strength equation;
- a failure equation; and
- an erosion equation for each constituent material.

These equations arise from the fact that, in general, the total stress tensor can be decomposed into a sum of a hydrostatic stress (pressure) tensor (which causes a change in the volume/density of the material) and a deviatoric stress tensor (which is responsible for the shape change of the material). An equation of state then is used to define the corresponding functional relationship between pressure, mass density and internal energy density (temperature). Likewise, a strength relation is used to define the appropriate equivalent plastic strain, equivalent plastic strain rate and temperature dependencies of the materials yield strength. This relation, in conjunction with the appropriate yield-criterion and flow-rule relations, is used to compute the deviatoric part of stress under elastic-plastic loading conditions. In addition, a material model generally includes a failure criterion (i.e. an equation describing the hydrostatic or deviatoric stress) and/or strain condition(s) which, when attained, cause the material to fracture and lose its ability to support (abruptly in the case of brittle materials or gradually in the case of ductile materials) tensile normal and shear stresses. Such failure criterion in combination with the corresponding material-property degradation and the flow-rule relations governs the evolution of stress during failure. The erosion equation is generally intended for eliminating numerical solution difficulties arising from highly distorted Lagrange cells (i.e. finite elements). Nevertheless, the erosion equation is often used to provide additional material failure mechanism especially in materials with limited ductility. To summarize, the equation of state along with the strength and failure equations (as well as with the equations governing the onset of plastic deformation and failure and the plasticity and failure induced material flow) enable assessment of the evolution of the complete stress tensor during a transient non-linear dynamics analysis. Such an assessment is needed where the governing (mass, momentum and energy) conservation equations are being solved. Separate evaluations of the pressure and the deviatoric stress enable inclusion of the non-linear shock effects (not critical, in the present work) in the equation of state.

Within the CU-ARL sand model, the equation of state is defined in terms of two relations:

- (1) a pressure vs density relations describing plastic compaction of sand under pressure; and
- (2) a sound speed vs density relation used to derive the pressure vs density relation during unloading or elastic reloading.

The strength component of the CU-ARL sand model also contains two functional relationships:

- (1) a shear modulus vs density relation governing (deviatoric) unloading/elastic-reloading response of sand; and

- 
- (2) a yield strength vs pressure relation describing the effect of pressure on the ideal plastic-shear response of sand.

A “hydro” type failure mode is assumed within the CU-ARL sand model. Consequently, failure occurs when pressure drops below a minimum (negative) pressure. “Failed” sand retains its ability to support pressure, retains a small fraction of its ability to support shear and completely loses its ability to support tensile stresses.

The erosion part of the CU-ARL sand model is defined in terms of a critical geometric instantaneous equivalent normal strain beyond which finite elements are removed from the model.

As stated earlier, a complete definition of all CU-ARL sand-model relations and the model parameterization can be found in Grujicic *et al.* (2007).

### 2.3 Finite element computational analysis

Once the geometrical/meshed models for the tire and sand bed as well as the material models for all the components of the tire and sand are defined, the finite element analysis of tire/sand interaction can be carried out by prescribing the appropriate initial and boundary conditions, to the tire and the sand bed and by defining the tire/sand contact surfaces and contact behavior. Toward that end the following steps are taken:

- (1) Zero-velocity initial conditions are prescribed to the entire model, i.e. both the tire and the sand bed are assumed to be initially at rest.
- (2) To prevent large-scale motion of the sand bed and to account for the confining effects of the surrounding sand, zero-velocity boundary conditions are prescribed to the sand bed four sides and its bottom.
- (3) The top side of the sand bed and the outer surfaces of the tire tread, carcass and sidewall are declared as contacting tire/sand surfaces.
- (4) A penalty algorithm is used to define these tire/sand normal contacts. Within this algorithm, high contact pressures are generated as a result of interpenetration/over-closure of the contacting surfaces. Also, a typical value (0.4) of tire/sand friction coefficient and a simple Coulomb friction model are used to account for frictional interactions between the tire and sand.
- (5) Modeling of the tire/sand interaction is divided into three steps:
  - tire inflation;
  - tire-deflection/sand indentation; and
  - tire rolling.

Within the inflation step, the internal pressure is increased from 0 kPa to the desired inflation pressure (between 140 and 250 kPa), in 0.25 s, while all degrees of freedom of the wheel-rim center are kept fixed. Within the second step, a vertical load is applied to the wheel-rim center in 0.5 s resulting in tire deflection and sand indentation. Within the third step, rolling of the tire is accomplished by prescribing the longitudinal velocity  $v_x$  and the lateral velocity  $v_y$  to the wheel-rim center. In addition, an angular velocity  $\omega$  is prescribed to the wheel-rim center around the  $y$ -direction. For a given level of longitudinal slip,  $I_x$ , the magnitude of  $\omega$  is determined from the following relation:

$$I_x = 1 - \left( \frac{v_x}{\text{re} \cdot \omega} \right) \quad (3)$$

where  $\text{re} = r_0 - \delta$  is the effective tire radius,  $r_0$  (0.3565 m) is the initial (i.e. zero vertical load) tire radius, while  $\delta$  is the vertical load-induced tire deflection determined in the second step. Within the third (0.5 s-long) step, the wheel is accelerated, from rest, at a constant linear acceleration over the first 0.4 s to attain a cruise velocity of 15 km/h. This was followed by a 0.1 s-long constant velocity travel of the wheel.

To attain the desired magnitude of slip angle,  $\alpha$ , the following relation is used to compute the required lateral velocity  $v_y$ , from the knowledge of the longitudinal velocity,  $v_x$ :

$$\alpha = \arctan \left( \frac{v_y}{v_x} \right) \quad (4)$$

Tire/sand interactions were studied under three vertical load levels (6,000, 8,000 and 10,000 N), nine longitudinal slip levels ( $-0.8, -0.6, -0.4, -0.2, 0.0, 0.2, 0.4, 0.6, 0.8$ ) and under nine levels of the slip angle ( $0^\circ, 2^\circ, 4^\circ, 6^\circ, 8^\circ, 10^\circ, 12^\circ, 14^\circ$  and  $16^\circ$ ).

It should be noted that step 1 analysis has to be run once for each level of the inflation pressure. (All the results reported in the next section were obtained at a constant level of inflation pressure of 200 kPa.) For each level of the inflation pressure, step 2 analysis has to be run once for each level of the wheel vertical force. The results obtained are next used as initial conditions to all step 3 analyses (each associated with different combinations of the longitudinal slip and the slip angle).

All the calculations carried out in this section were done using ABAQUS/Explicit (Dassault Systems, 2008), a general purpose non-linear dynamics modeling and simulation software. In the remainder of this section, a brief overview is given of the basic features of ABAQUS/Explicit, emphasizing the aspects of this computer program which pertain to the problem at hand.

A transient non-linear dynamics problem is analyzed within ABAQUS/Explicit by solving simultaneously the governing partial differential equations for the conservation of momentum, mass and energy along with the materials' constitutive equations and the equations defining the initial and the boundary conditions. The equations mentioned above are solved numerically using a second-order accurate explicit scheme and one of the two basic mathematical approaches, the Lagrange approach and the Euler approach. The key difference between the two approaches is that within the Lagrange approach the numerical grid is attached to and moves along with the material during calculation, while within the Euler approach, the numerical grid is fixed in space and the material moves through it. Within ABAQUS/Explicit, the Lagrange approach is used. In Grujicic *et al.* (2007), a brief discussion was given of how the governing differential equations and the materials' constitutive models define a self-consistent system of equations for the dependent variables (nodal displacements, nodal velocities, element material densities and element internal energy densities).

### 3. Results and discussion

In this section and its sub sections, the main results obtained in the present work are presented and discussed.



### 3.1 Validation of the tire model

As discussed earlier, to validate the tire model a multi-step computational analysis of tire contact and rolling over a rigid-road surface was first investigated. The analysis included tire inflation, bringing the tire in contact with the road, application of the vertical load and tire rolling (the wheel's center point was translated while allowing it to freely rotate about its axis due to friction, simulating a "towed-wheel" case). The tire/road contact was assumed to be frictionless during the loading step, and friction was added during the rolling step. During the rolling/towing step, the tire was accelerated from rest to 1 m/s at a constant acceleration of 1 m/s<sup>2</sup> for 1 s and then it was allowed to roll at a constant velocity of 1 m/s for two more seconds.

A comparison of the computed and measured tire deflection results when placed in contact with a rigid-road surface and subjected to different vertical loads (from 0 to 8,000 N) at three inflation pressures (241 kPa/35 psi, 179 kPa/26 psi and 138 kPa/15 psi) is shown in Figure 2(a). The suggested inflation pressure for the tire is 241 kPa. Lower inflation pressures are sometimes used to reduce the wheel sinkage when driving in off-road conditions and for minimizing damage to unpaved travel surfaces. Consequently, the two lower inflation pressures were also evaluated. Performance at a range of inflation pressures is also of interest to industries using vehicles with central tire inflation systems (i.e. military, forestry and agriculture). The results shown in Figure 2(a) show that the model predictions agree quite well with the experimental data reported in Shoop (2001) for all three tire pressures investigated.

A comparison between the model predicted and the measured tire contact area results is shown in Figure 2(b). The contact areas are based on the perimeter of the contact, without accounting for voids within the area due to tread design. In general, the agreement between the model and the measured data is quite good.

The distributions of the contact stresses over the contact patch area at different vertical loads and inflation pressures were also determined in the present work and the results were compared with their experimental counterparts as reported in Shoop (2001). Both the computed and the measured results revealed high stress values at the tire shoulder and, to a lesser extent, along the tire centerline. The overall computation/experiment agreement was quite good. Owing to copyright restrictions, the measured contact stress distribution results could not be reproduced here and, hence, the corresponding computed results are also omitted.

As far as the tire-rolling step computational results are concerned, they were found to yield comparable values for the hard-surface rolling resistance when compared to the corresponding experimental data (Shoop, 2001). For example, at a tire/road friction coefficient of 0.825 (consistent with the case of an asphalt pavement), an inflation pressure of 241 kPa and a tire velocity of 8 km/h, the computed rolling-resistance was ca. 23 N, while the corresponding experimental values were around 25 N (Shoop, 2001). This finding suggests that energy dissipation associated with visco-elastic behavior of rubber compounds in the tire (accounted for in the present model) makes a major contribution to the tire hard-surface rolling resistance.

Based on the results presented and discussed in this section, it was concluded that the present finite element model for the Goodyear Wrangler HT tire is a good compromise between physical reality and computational efficiency.

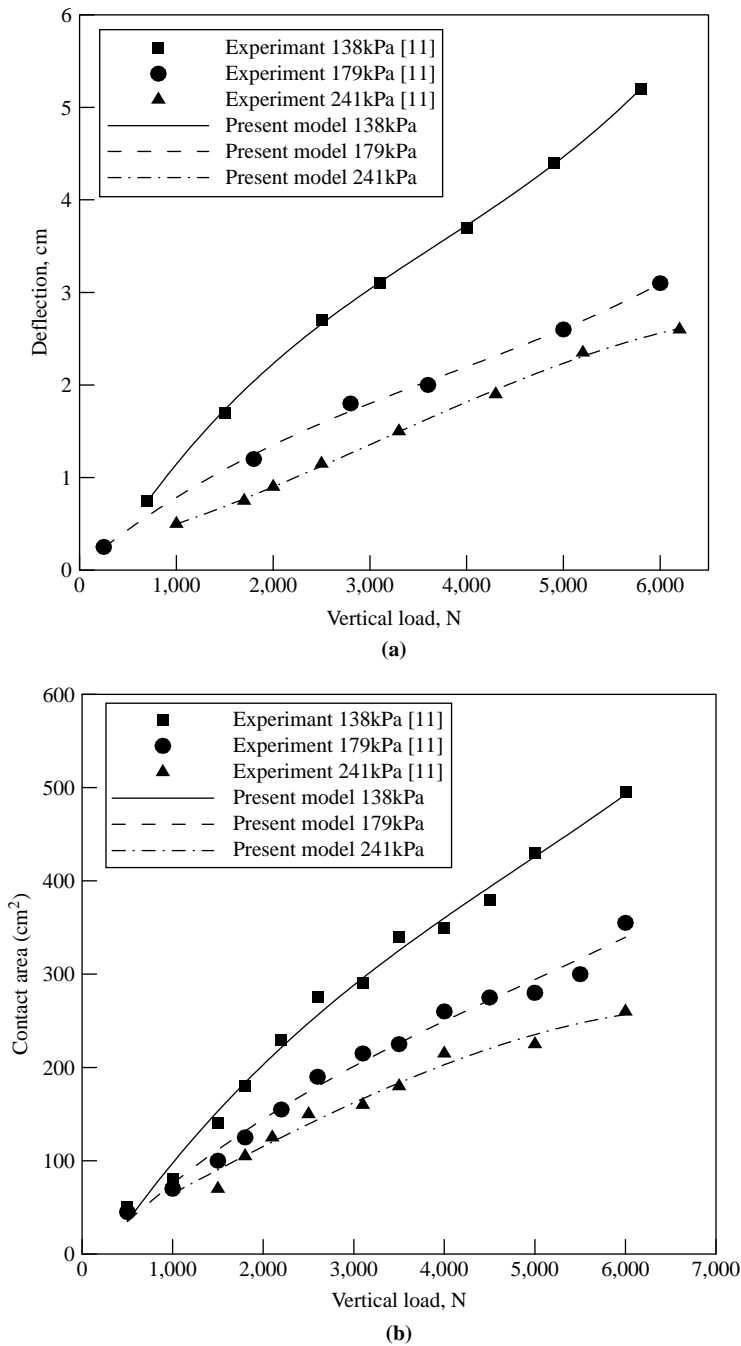


**Figure 2.** The effects of vertical load and tire inflation pressure on the (a) deflection and (b) contact-patch size for a Goodyear Wrangler HT tire in contact with a hard-road surface

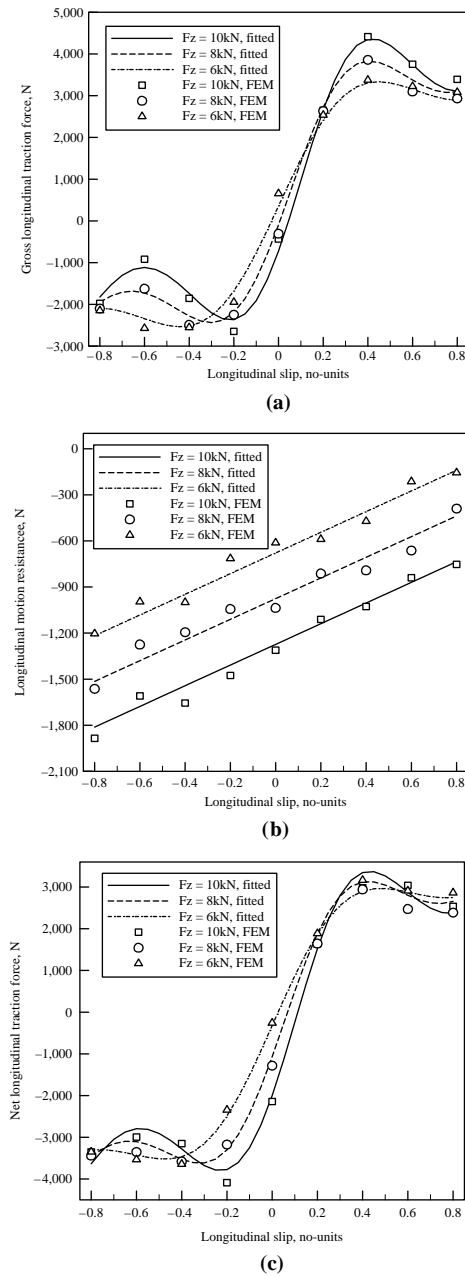
### 3.2 Tire/sand interactions: pure longitudinal slip case

In this section, the results of the finite element investigation of the tire rolling in sand under pure longitudinal slip conditions (i.e. at a zero slip angle) are first presented and discussed. Then, the results are combined with the so-called Pacejka “Magic Formula” tire model (Pacejka, 1966) and an engineering design optimization procedure to define and parameterize the relations between the gross longitudinal traction force (i.e. the traction effort),  $F_x$ , the corresponding longitudinal motion resistance,  $R_x$ , and the net longitudinal traction force (i.e. the drawbar pull),  $P_x$ , as dependent variables and the longitudinal slip,  $I_x$ , and the vertical force,  $F_z$ , as independent variables.

The effect of the longitudinal slip,  $I_x$ , as defined in equation (3), in a range between  $-0.8$  and  $0.8$  at three levels of vertical loads (6,000, 8,000 and 10,000 N) and inflation/contact pressure of 200 kPa on the gross longitudinal traction force,  $F_x$ , is shown in Figure 3(a). The corresponding results for the tire longitudinal rolling resistance,  $R_x$ , and the net longitudinal traction force,  $P_x$ , are shown in Figure 3(b) and (c), respectively. A brief examination of the results shown in Figure 3(a)-(c) reveals that:

- The effect of the longitudinal slip,  $I_x$ , on the gross longitudinal traction force,  $F_x$  (Figure 3(a)), shows the behavior which is normally observed in the case of tire/rigid-road interactions. That is, the  $F_x$  vs  $I_x$  relation is fairly linear in a region around  $I_x = 0$ , then becomes non-linear, goes through an extreme value and then decreases monotonically or in an oscillatory manner. However, unlike the case of tire/rigid-road interactions where  $F_x = 0$  (or nearly zero) under the pure rolling condition, the longitudinal gross traction is non-zero at  $I_x = 0$ . This finding is consistent with the fact that, in order to maintain forward traction at  $I_x = 0$ , the  $F_x$  must be able to overcome the effect of the longitudinal motion resistance,  $R_x$ , Figure 3(b).
- The effect of the vertical force,  $F_z$ , on the magnitude of the gross longitudinal traction force,  $F_x$ , is quite complex and is greatly affected by the value of the longitudinal slip  $I_x$  (Figure 3(a)).
- The effect of both the longitudinal slip,  $I_x$ , and the vertical force,  $F_z$ , on the longitudinal motion resistance,  $R_x$ , is fairly monotonic. The vertical force is found to increase the magnitude of the motion resistance at all levels of the longitudinal slip,  $I_x$ . Interestingly,  $R_x$  was found to increase in magnitude with an increase in the longitudinal slip,  $I_x$ . This finding was found to be related to an accompanying reduction in the wheel sinkage. That is, as  $I_x$  is increased, the wheel sinkage is found to decrease, requiring less sand to be compacted by the rolling tire.
- The effect of the vertical force and the longitudinal slip on the net longitudinal traction force (i.e. drawbar pull) is simply a combination of these two parameters on the gross longitudinal traction force and on the longitudinal motion resistance, since  $P_x = F_x + R_x$ .

Since one of the main objectives of the present work is to derive the functional relationships for the tire/sand interactions which can be used in multi-body dynamics simulations of the off-road vehicle performance, an attempt is made in the remainder of this section to derive such functions which relate the gross longitudinal traction force,  $F_x$ , the longitudinal motion resistance,  $R_x$ , and the net longitudinal traction force,  $P_x$ , to the vertical force,  $F_z$ , longitudinal slip,  $I_x$ , and the tire/sand friction coefficient,  $\mu$ .



**Notes:** (a) The gross longitudinal traction force (i.e. the traction effort),  $F_x$ ; (b) the longitudinal motion resistance force,  $R_x$ ; (c) the net longitudinal traction force (i.e. the drawbar pull),  $P_x$

**Figure 3.**  
The effect of the vertical load,  $F_z$ , and the longitudinal slip,  $I_x$

Considering the fact that, for pneumatic tires, the gross longitudinal traction force which describes longitudinal tire dynamic behavior during rolling on a non-deformable road is represented using the so-called Pacejka “Magic Formula” tire model (Pacejka, 1966), the same functional relationship is adopted in the present work. Over the last 20 years, (Pacejka, 1966, 2002; Pacejka and Besselink, 2008) has developed a series of tire models. These models are generally named the “Magic Formula” mainly to denote that while there is no particular physical basis for the mathematical expressions/equations used in the models, they fairly well account for the dynamic behavior of a wide variety of tire designs/constructions and operating conditions. Within the magic formula, each important tire force/moment is represented by an equation containing between ten and 20 parameters. Among these forces/moments are the longitudinal and the lateral slip forces, and self-aligning torque (the torque that a tire creates as it is steered, i.e. rotated around its vertical axis). The Pacejka magic formula tire model parameters are typically determined by applying non-linear regression (i.e. curve fitting) to experimental data.

The official Pacejka-96 magic formula (Pacejka, 2002; Pacejka and Besselink, 2008) for the gross longitudinal traction force is defined as follows:

$$F_x = D \sin(C \tan(B(1 - E)(I_x + Sh) + E \tan^{-1}(B(I_x + Sh)))) + S_v \quad (5)$$

where  $C = a_0$ ,  $D = (a_1 F_z + a_2) F_z$  ( $a_2$  is the friction coefficient multiplied by a factor of 1,000),  $B = ((a_3 F_{z2} + B_4 F_z) \exp(-a_5 F_z)) / CD$ ,  $E = a_6 F_{z2} + a_8$ ,  $Sh$ ,  $S_v$  and  $F_z$  is the normal force. The parameters  $C$ ,  $D$ ,  $Sh$  and  $S_v$  have the following physical meaning:  $C$  is the factor which determines the shape of the  $F_x$  vs  $I_x$  curve peak,  $D$  is the peak  $F_x$  value (except for the motion-resistance-controlled vertical shift,  $S_v$ ),  $Sh$  is the motion-resistance-controlled longitudinal slip shift.

The official Pacejka-96 magic formula, equation (5), contains ten longitudinal traction force parameters:  $a_0$ – $a_1$ ,  $a_3$ – $a_8$ ,  $Sh$  and  $S_v$ . Despite a relatively large number of parameters, the initial attempts to fit the results shown in Figure 3(a) using equation (5) were not successful. Hence, equation (5) was expanded by modifying the following terms as:

- $D = (a_1 F_z + a_2) F_z + a_9$ .
- $B = ((a_3 F_{z2} + B_4 F_z + a_{10}) \exp(-a_5 F_z - a_{11})) / CD$ .
- $Sh = Sh_1 + Sh_2 F_z$ .
- $S_v = S_{v1} + S_{v2} F_z$ .

It is critical to recognize that due to the modifications of equation (5), listed above, the new  $F_x$  vs  $I_x$  relation does not yield  $F_x = 0$  at  $F_z = 0$ . Hence, the application range of the modified  $F_x$  vs  $I_x$  relation is limited to the  $F_z \gg 0$  region; and, for good accuracy, only to the 6,000-10,000 N,  $F_z$  range.

The modified Pacejka-96 magic formula thus contains 15 parameters  $a_0$ – $a_1$ ,  $a_3$ – $a_{11}$ ,  $Sh_1$ ,  $Sh_2$ ,  $S_{v1}$  and  $S_{v2}$  which were determined in the present work by fitting the finite element-based  $F_x$  vs  $I_x$  results shown in Figure 3(a), to the modified Pacejka magic formula equation (5).

Owing to the high non-linearity of the functional relation described in equation (5) and uncertainties regarding the order or values of the unknown parameters, computationally efficient gradient-based optimization algorithms (e.g. the conjugate

gradient method) which are generally capable of finding only a local minimum were not used. Instead, a global optimization algorithm, the genetic algorithm (Goldberg, 1989), was employed in order to search a large domain in the unknown parameter design space. The objective function used in the optimization procedure was defined as a negative sum of squares of the differences in  $F_x$  values predicted by equation (5) and their counterparts obtained using the finite element computational procedure. Optimization (i.e. finding the maximum of the objective function) was carried out in the absence of any constraints. A brief description of the genetic algorithm (Goldberg, 1989) used in the present work is provided in the Appendix.

The outcome of the aforementioned parameter determination procedure is summarized in Table I. The goodness-of-fit of the  $F_x$  vs  $I_x$  relations predicted by equation (5) and its parameterization given in Table I at three different values of  $F_z$  can be seen in Figure 3(a) in which the finite element results are displayed as discrete symbols, while the fitting curves are shown as lines.

The longitudinal motion resistance,  $R_x$ , vs the longitudinal slip,  $I_x$ , results at different levels of the vertical force,  $F_z$ , shown in Figure 3(b), are fitted to a bi-linear function in the force  $R_x(N) = aR_x + bR_xI_x + cR_xF_z(kN)$ . Using a simple linear regression analysis the three parameters in the relation are determined as:  $aR_x = 215.31$ ,  $bR_x = -148.89$  and  $cR_x = 673.07$ . The outcome of this curve fitting procedure can be seen in Figure 3(b) in which the finite element results are displayed as discrete symbols, while the fitting function is represented as lines.

Since the net longitudinal traction force,  $P_x$ , is a difference between the gross longitudinal traction force and the longitudinal motion resistance force and the latter two have already been parameterized, no curve-fitting/parameterization procedure had to be applied to the  $P_x$  vs  $I_x$  relationship under different  $F_z$  levels. The goodness-of-fit for the  $P_x$  vs  $I_x$  function is shown in Figure 3(c) in which the finite element results are displayed as discrete symbols while the fitting function is shown using lines.

Parameter	Unit	Value
$a_1$	1/MN	- 4.6838
$a_2$	1/k	- 33.331
$a_3$	1/MN	39,367
$a_4$	1/k	$1.319 \times 10^5$
$a_5$	1/kN	0.11878
$a_6$	1/(kN) <sup>2</sup>	- 0.012162
$a_7$	1/kN	- 3.213
$a_8$	N/A	74.286
$a_9$	N	- 2,567.3
$a_{10}$	N	$- 1.5557 \times 10^5$
$a_{11}$	N/A	9.0708
C	N/A	23.568
$S_{h1}$	N/A	- 14.409
$S_{h2}$	1/kN	2.4581
$S_{v1}$	N	- 496.49
$S_{v2}$	1/k	149.1

**Table I.**  
Parameterization of the functional relationship between the tire/sand gross longitudinal force,  $F_x$  (N), the longitudinal slip,  $I_x$  (%) and the vertical force,  $F_z$  (kN), as defined in equation (5)

### 3.3 Tire/sand interactions: combined longitudinal/lateral slip case

In this section, the results of the finite element investigation of the tire rolling in sand under combined longitudinal/lateral slip conditions are first presented and discussed. Then, the results are subjected to the optimization procedure described in the previous section in order to define and parameterize the relations between the gross lateral traction force,  $F_y$ , the corresponding lateral motion resistance,  $R_y$ , and the net lateral traction force,  $P_y$ , as dependent variables and the slip angle,  $\alpha$ , and the vertical force,  $F_z$ , as independent variables (under a pure rolling condition).

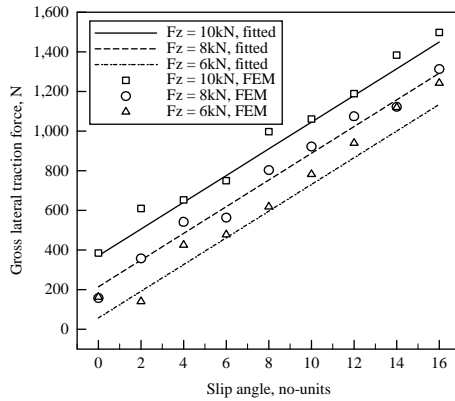
The effect of the slip angle in a range between  $0^\circ$  and  $16^\circ$  at three levels of vertical loads (6,000, 8,000 and 10,000 N), inflation pressure of 200 kPa and a zero value of the longitudinal slip on the gross lateral traction force,  $F_y$ , are shown in Figure 4(a). The corresponding results for the lateral rolling resistance,  $R_y$ , and the net lateral traction force,  $P_y$ , are shown in Figure 4(b) and (c), respectively. A brief examination of the results shown in Figure 4(a)-(c) reveals that:

- The lateral gross traction force,  $F_y$ , increases with both an increase in the slip angle,  $\alpha$ , and an increase in the vertical force,  $F_z$  (Figure 4(a)). These results are quite expected since a larger  $\alpha$  and higher value of  $F_z$  both give rise to a larger amount of sand that has to be ploughed during lateral motion of the wheel.
- The aforementioned effects of the increased  $\alpha$  and  $F_z$  are also directly reflected in Figure 4(b), in which the effect of these parameters on the lateral motion resistance  $R_y$  is displayed.
- The effects of  $\alpha$  and  $F_z$  on the net lateral traction force  $P_y$  are natural consequences of the effects of these two parameters on  $F_y$  and  $R_y$ .

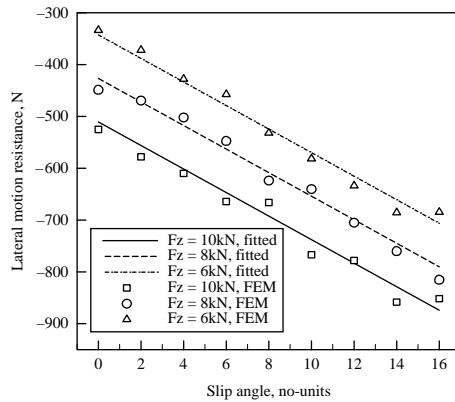
While there is a Pacejka magic formula for the gross traction force,  $F_y$ , similar to that one shown in equation (5), the results shown in Figure 4(a) revealed that a simpler  $F_y$  vs  $\alpha$  relation at different  $F_z$  values can be used. In fact, a bi-linear relation in the form:  $F_y(\text{N}) = aF_y + bF_y\alpha(\text{deg}) + cF_yF_z(\text{kN})$  has been found to quite realistically account for the results shown in Figure 4(a). The linear multiple regression analysis mentioned earlier resulted in the following values of  $F_y$  parameters:  $aF_y = 413.4$ ;  $bF_y = -78.462$ ;  $cF_y = -67.371$ . The goodness-of-fit for the  $F_y$  vs  $\alpha$  function is shown in Figure 4(a) in which the finite element results are displayed as discrete symbols, while the fitting function is shown as lines.

The results shown in Figure 4(b) are also fitted to a bi-linear relation in the form:  $R_y(\text{N}) = aR_y + bR_y\alpha(\text{deg}) + cR_yF_z - (\text{kN})$ . The aforementioned linear multiple regression analysis yielded:  $aR_y = 278.82$ ;  $bR_y = -41.945$ ;  $cR_y = -22.718$ . The goodness-of-fit for the  $R_y$  vs  $\alpha$  function is shown in Figure 4(b) in which the finite element results are displayed as discrete symbols, while the fitting function is shown as lines.

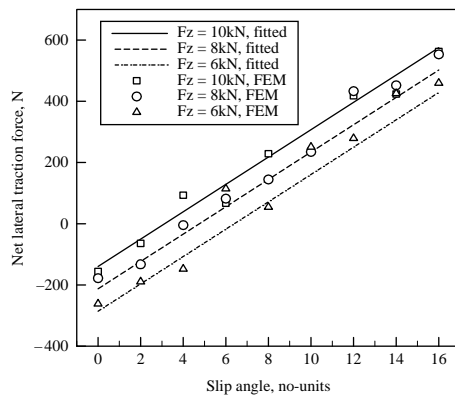
The  $P_y$  vs  $\alpha$  results at different values of the vertical force,  $F_z$  (Figure 4(c)), were fitted by simply combining the parameters of the  $F_y$  and  $R_y$  functions. Since  $P_y = F_y + R_y$ . The goodness-of-fit for the  $P_y$  vs  $\alpha$  function is shown in Figure 4(c) in which the finite element results are displayed as discrete symbols while the fitting function is shown as lines.



(a)



(b)



(c)

**Notes:** (a) The gross lateral traction force,  $F_y$ ; (b) the lateral motion resistance force,  $R_y$ ; (c) the net lateral traction force,  $P_y$

**Figure 4.**  
The effect of the vertical load,  $F_z$ , and the slip angle,  $\alpha$



### 3.4 Spatial distribution of the tire/sand contact stresses

In order to provide some rationale for the observed effects of the tire/sand interaction conditions (i.e. longitudinal slip, slip angle and vertical force) on the observed traction and resistance forces, a brief investigation of the distribution of the normal and shear contact stresses over the tire/sand contact patch is investigated in the present section. Owing to space limitations, only the pure longitudinal case is considered. Furthermore, only two longitudinal slip conditions are considered:

- (1)  $I_x = -0.4$  which corresponds to the so-called “braked-wheel” ( $F_x < 0$ ) condition; and
- (2)  $I_x = 0.4$  which corresponds to the so-called “driving wheel” ( $P_x > 0$ ) condition.

Also, only case of the vertical force  $F_z = 10,000$  N and inflation pressure  $P = 200$  kN are considered.

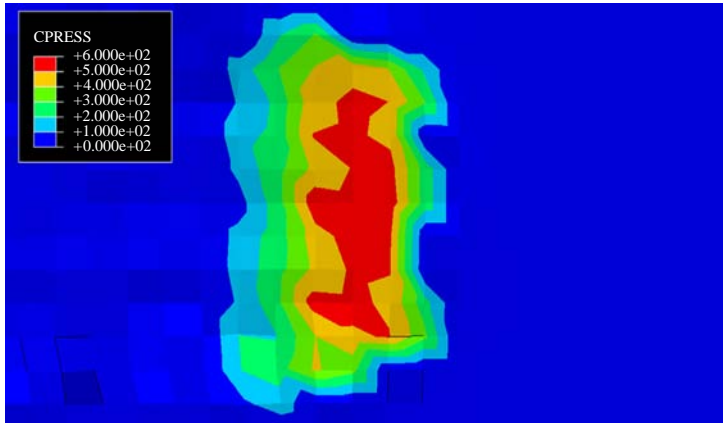
A typical example of the spatial distribution of the normal contact pressure and the shear contact stress over the tire/sand contact patch in the case of the “braked wheel” is shown in Figure 5(a) and (b), respectively. Likewise, a typical spatial distribution of the normal contact pressure and the shear contact stress over the tire/sand contact patch in the case of the “driving wheel” is shown in Figure 6(a) and (b). The results displayed in these figures can be summarized as follows:

- The highest levels of the contact pressure are seen, as expected, at the portions of the contact patch where the treads are making deep indentations in the sand (Figures 5(a) and 6(a)).
- Owing to forward slip and the accompanying additional wheel sinkage, higher contact pressures are seen in the braked-wheel case (Figure 5(a)) than in the driving-wheel case (Figure 6(a)).
- In the driving-wheel case of Figure 6(b), only negative contact shear stresses are seen over the contact patch. These stresses are the origin of the tire/sand traction and responsible for the forward motion of the wheel. In sharp contrast, and as expected, in the braked-wheel case (Figure 5(b)), the contact shear stresses are both negative (forward-motion promoting) and positive (lead to deceleration of the wheel and its ultimate stoppage).

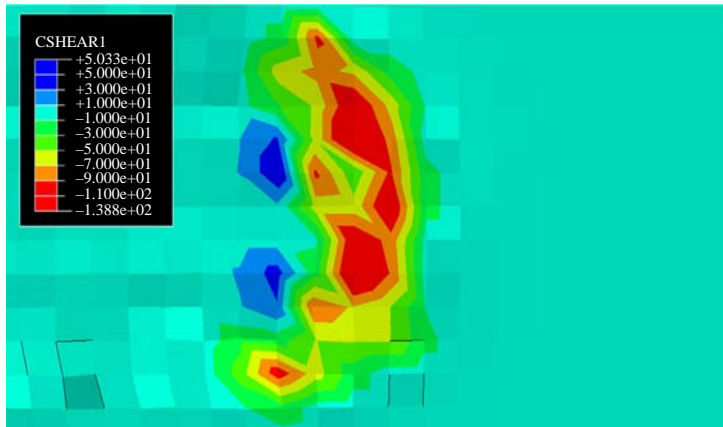
The results presented and discussed in this section provide a qualitative evidence for relationships between the tire/sand contact phenomena/stresses and the resulting traction/motion-resistance forces. A more comprehensive and quantitative investigation of these relationships is underway (Grujicic *et al.*, 2009b) and will be reported in our future communication.

### 3.5 Implementation and validation of the tire/sand interaction model

To validate the tire/sand interaction model derived in the present work, the model and its new parameterization given in Sections 3.2 and 3.3 and in Table I are first implemented in SIMPACK, a general purpose multi-body dynamics program (Intec Inc., 2008). This was done via the “*utyre\_spck.f*” user tire model subroutine. Within this subroutine, the current values of the wheel center kinematic parameters (e.g. vertical displacement, longitudinal displacement, rotational speed around the wheel axis, etc.)



(a)



(b)

**Figure 5.**  
Spatial distribution of:  
(a) the normal and (b) the  
shear stresses over the  
tire/sand contact patch for  
the pure-longitudinal  
“braked-wheel”  
( $I_x = -0.5$ ) case, the  
vertical force of 10,000 N  
and inflation pressure  
of 200 kN

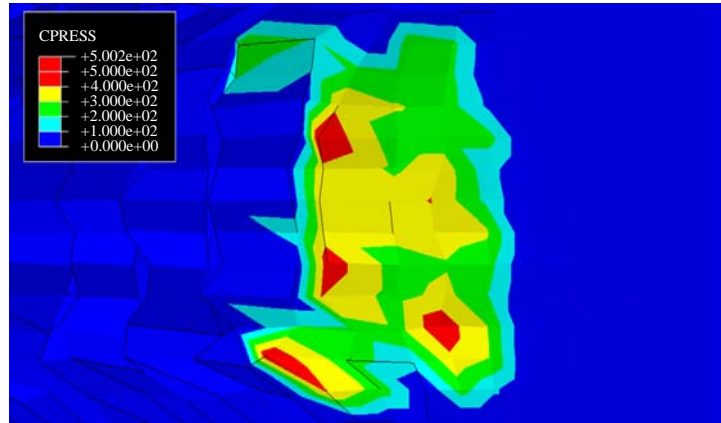
are used to calculate the vertical force, the, longitudinal slip, the longitudinal gross and net traction forces, etc.

Since full validation of the tire/sand interaction model derived in the present work is the subject of an ongoing investigation (Grujicic *et al.*, 2009b), only a couple of preliminary results is presented and discussed in the remainder of this section.

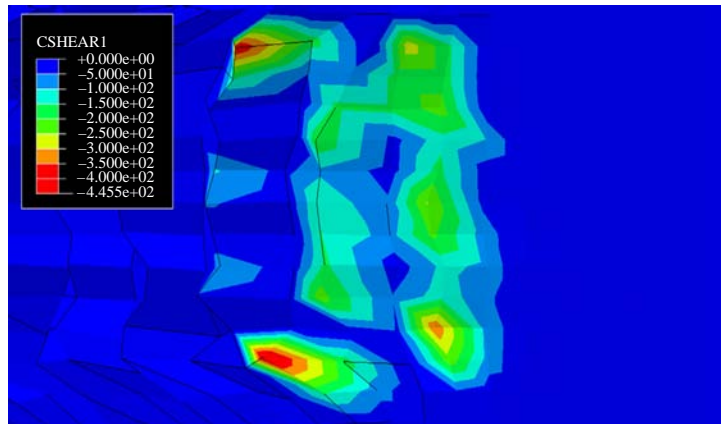
To validate the present tire/sand interaction model and the resulting force element, parallel finite element and multi-body dynamics investigations are carried out of two types of flatland braking maneuvers:

- (1) straight line braking; and
- (2) braking while making a turn (“curve braking”).

Typical material distribution configurations obtained in the finite element analyses of the two braking maneuvers are shown in Figure 7(a) and (b).



(a)

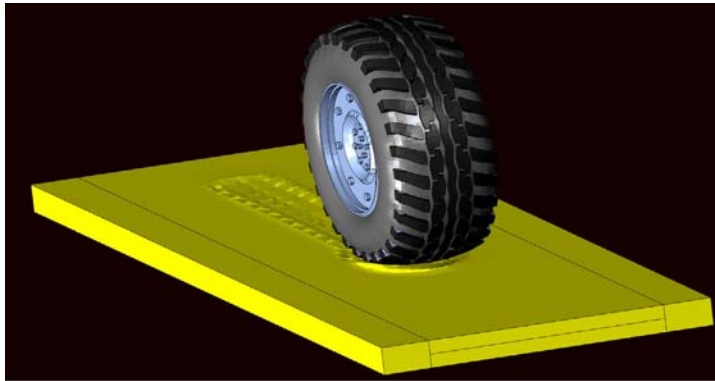


(b)

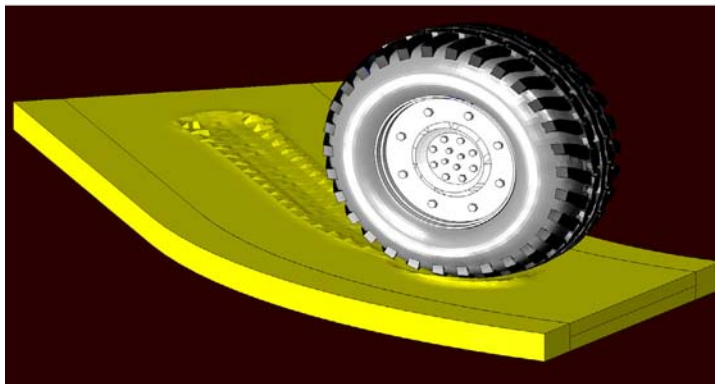
**Figure 6.** Spatial distribution of:  
(a) the normal and  
(b) the shear stresses over  
the tire/sand contact patch  
for the pure-longitudinal  
“driving-wheel” ( $I_x = 0.5$ )  
case, the vertical force  
of 10,000 N and inflation  
pressure of 200 kN

In Figure 8(a), a comparison is made between the braking distance vs braking torque results obtained using the finite element analysis and the multi-body dynamics analysis. It is obvious that the two sets of results are in fairly good agreement, suggesting that, at least under pure longitudinal conditions of straight line flat land braking, the present tire/sand interaction when implemented as a force element in a multi-body dynamics model yields the results which are in full agreement with a more rigorous (yet computationally quite more expensive) finite element calculations. It should be also noted that the results shown in Figure 8(a) show that under very severe braking conditions (i.e. under large braking torque conditions), extensive forward slip can give rise to an increase in the braking distance.

Figure 8(b) shows a comparison between the finite element and multi-body dynamics-based results pertaining to the effect of braking torque on the braking distance during a (10m radius of curvature) curve flatland braking maneuver.



(a)



(b)

Notes: (a) Straight line flatland braking; (b) curve flatland braking maneuvers

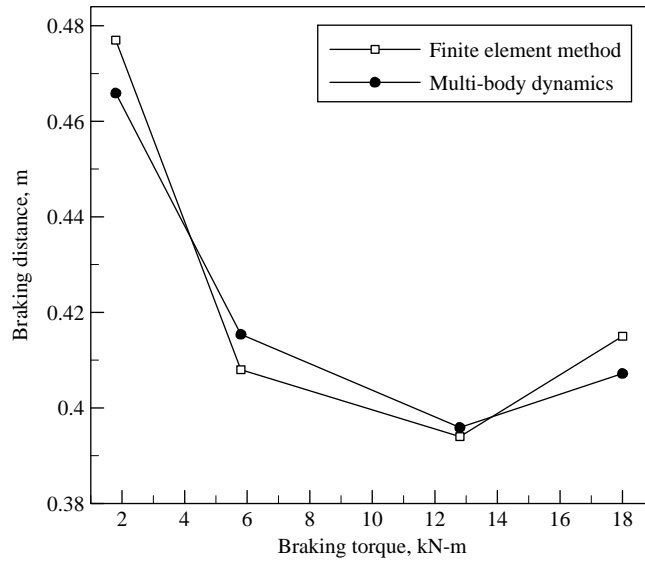
**Figure 7.**  
Typical tire/sand material  
distributions obtained  
during the finite element  
analyses

Again, agreement between the two sets of results is reasonably good. Based on these results, it is concluded that even under combined longitudinal/lateral conditions, the present tire/sand interaction model is quite reasonable. As stated earlier, more extensive and thorough validation of this model is underway (Grujicic *et al.*, 2009b).

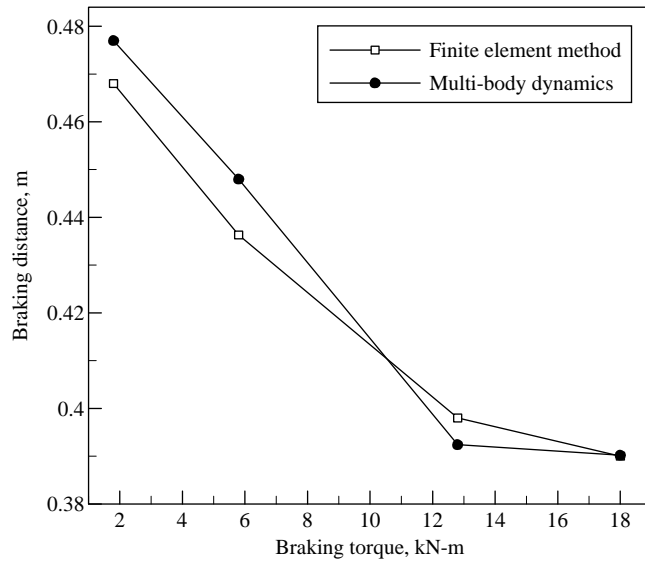
#### 4. Summary and conclusions

Based on the results obtained in the present work, the following main summary remarks and conclusions can be drawn:

- A series of finite element computational analyses is carried out in order to investigate rolling/slip behavior of a prototypical pneumatic tire in sand under various conditions of inflation pressure, vertical force, longitudinal slip and slip angle.
- The results obtained are used to construct mathematical functions relating the longitudinal and lateral gross traction forces, the motion-resistance forces and the



(a)



(b)

**Figure 8.**  
A comparison between the braking distance vs braking torque results obtained during a finite element analysis and a multi-body dynamics analysis

**Notes:** (a) Straight line flatland braking; (b) curve flatland braking maneuvers

---

net traction forces as dependent variables as functions of the vertical force, longitudinal slip and slip angle, as independent variables.

- To validate the newly derived tire/sand interaction model, the aforementioned functional relationships are implemented in a general-purpose multi-body dynamics code. By comparing the results obtained using the finite element analysis and the corresponding multi-body dynamics computations of simple flatland straight line and curve maneuvers, it was established that the present tire/sand interaction model when implemented as a force element in a multi-body dynamics model accounts fairly well for the expected off-road wheel behavior both under pure-longitudinal and combined longitudinal/lateral conditions.

## References

- Arons, E.M. and Colbeck, S.C. (1995), "Geometry of heat and mass transfer in dry snow – a review of theory and experiment", *Reviews of Geophysics.*, Vol. 33 No. 4, pp. 463-93.
- Bekker, G. (1956), *Theory of Land Locomotion*, The University of Michigan Press, Ann Arbor, MI.
- Bekker, G. (1960), *Off-road Locomotion*, The University of Michigan Press, Ann Arbor, MI.
- Bekker, G. (1969), *Introduction to Terrain-Vehicle Systems*, The University of Michigan Press, Ann Arbor, MI.
- Clark, S.K. (1981), *Mechanics of Pneumatic Tires*, US Department of Transportation, National Highway Traffic Safety Administration, Washington, DC.
- Dassault Systems (2008), *ABAQUS Version 6.8.1, User Documentation*, Dassault Systems, Providence, RI.
- Goldberg, D.E. (1989), *Genetic Algorithms in Search. Optimization and Machine Learning*, Addison-Wesley, Reading, MA.
- Grujicic, M., Arakere, G., Bell, W.C. and Haque, I. (2009a), "Computational investigation of the effect of up-armoring on occupant injury/fatality reduction of a prototypical high-mobility multi-purpose wheeled vehicle subjected to mine-blast", *Journal of Automobile Engineering*, Vol. 223, pp. 903-20.
- Grujicic, M., Bell, W.C., Arakere, G. and Haque, I. (2009b), "Finite element analysis of the effect of up-armoring on the off-road braking and sharp-turn performance of a high-mobility multi-purpose wheeled vehicle (HMMWV)", *Journal of Automobile Engineering*, Vol. 223, D11, pp. 1419-34.
- Grujicic, M., Pandurangan, B., Haque, I., Cheeseman, B.A. and Skaggs, R.R. (2007), "A computational analysis of mine blast survivability of a commercial vehicle structure", *Multidiscipline Modeling in Materials and Structures*, Vol. 3, pp. 431-60.
- Intec (2008), *SIMPACK Version 8900, User Documentation*, Intec, Indianapolis, IN.
- Lee, J. and Kiu, Q. (2007), "Modeling and simulation of in-plane and out-of-plane forces of pneumatic tires on fresh snow based on the finite element method", *Proceedings of the Joint North America, Asia-Pacific ISTVS Conference and Annual Meeting of Japanese Society for Terramechanics, University of Alaska, Fairbanks, AK*.
- Pacejka, H.B. (1966), "The wheel shimmy phenomenon: a theoretical and experimental investigation with particular reference to the nonlinear problem (analysis of shimmy in pneumatic tires due to lateral flexibility for stationary and non-stationary conditions)", PhD thesis, Delft University of Technology, Delft.
- Pacejka, H.B. (2002), *Tire and Vehicle Dynamics*, Butterworth-Heinemann, Oxford.

- Pacejka, H.B. and Besselink, I.J.M. (2008), "Magic formula tire model with transient properties", *Supplement to Vehicle System Dynamics*, Vol. 27, pp. 234-49.
- SAE (1992), *SAE Glossary of Automotive Terms*, Society of Automotive Engineers, Warrendale, PA.
- Shoop, S.A. (2001), "Finite element modeling of tire-terrain interaction", CRREL Technical Report, ERDC/CRREL TR-01-16, US Army Cold Regions Research and Engineering Laboratory, Hanover, NH.
- Shoop, S.A., Kestler, K. and Haehnel, R. (2006), "Finite element modeling of tires on snow", *Tire Science and Technology*, Vol. 34 No. 1, pp. 2-37.
- Wong, J.Y. (1989), *Terramechanics and Off-road Vehicles*, Elsevier, New York, NY.
- Yong, R.N., Fattah, E.Z. and Skiadas, N. (1984), *Vehicle Terrain Mechanics*, Elsevier, New York, NY.

#### **Appendix. Genetic algorithm for parameterization of the tire/sand model**

In this section, a brief description is given of the optimization procedure used to determine the unknown parameters in the Pacejka (1966) magic formula for the tire/sand gross longitudinal traction force as a function of the longitudinal slip. The unknown parameters must be selected so that the deviation of the gross longitudinal traction force predicted by the magic formula from its counterpart computed in the present work using the finite element procedure described in the previous sections is minimal over a wide range of normal forces and the entire range of the longitudinal slip. The question then becomes how to efficiently search the model parameter space for the values which give rise to a global maximum in the objective function (defined as a negative sum of squared differences between the values of the tire/sand gross longitudinal traction force predicted by the Pacejka magic formula and by the finite element method).

A review of the literature identifies three main types of search methods:

- (1) calculus-based;
- (2) enumerative; and
- (3) random methods.

While generally very fast, calculus-based methods suffer from two main drawbacks:

- (1) they are local in scope, i.e. they typically locate the maximum which is highest (best) in the neighborhood of the current search point; and
- (2) they entail the knowledge of derivatives of the objective function whose evaluation (even through the use of numerical approximations) in multi-modal and potentially discontinuous search spaces represents a serious limitation.

Within enumerative search methods, values of the objective function are evaluated at every pre-selected point in the research space, one at a time. These methods generally require evaluation of the objective function at a large number of pre-selected points which tends to make them inefficient and not very useful for problems of even moderate size and complexity.

Owing to the aforementioned shortcomings of the calculus-based and enumerative search methods, the genetic algorithm (Goldberg, 1989), one of the random search methods, is used in the present work. Through (binary) coding, the genetic algorithm creates a parameter string (a chromosome set) for each considered point (individual) in the search space and utilizes the Darwinian principle of "Survival of the Fittest" to ensure that chromosomes of the fittest individuals are retained (with a higher probability) in subsequent generations.

At the beginning of the genetic algorithm search procedure, a random selection of the parameters is used to create an initial population of individuals (parameter sets) of size  $n$  in the search space. The fitness (i.e. the objective function) is next computed for each of the individuals

based on how well each individual performs (in its environment). To generate the next generation of individuals of the same population size, the genetic algorithm performs the following three operations:

- (1) selection;
- (2) crossover; and
- (3) mutation.

Within the selection process, fitter individuals are selected (as parents) for mating, while weak individuals die off. Through mating, the parents create a child with a chromosome set that is some mix of the parents' chromosomes. Mixing of parents' chromosomes during child creation is referred to as crossover. To promote evolution, a small probability is used to enable one or more child's chromosomes to mutate (change). The process of child creation and mutation are continued until an entirely new population (of children) of size  $n$  is generated. The fitness of each child is determined and the processes of selection, crossover and mutation repeated resulting in increasingly fitter generations of individuals. A logic flow chart of the genetic algorithm is shown in Figure A1. Few important details regarding parameter coding, selection, crossover and mutation are given below:

- *Binary parameter coding.* The total number of possible equally spaced values of each parameter (within the selected range) is first defined. The number of possible values is typically set to  $2^{nm}$ , where nanometer is a positive integer. Each possible value of a parameter is next coded using a binary format. For example, when the total number of possible values of a parameter is  $215 = 32,768$ , that parameter is coded using a string of

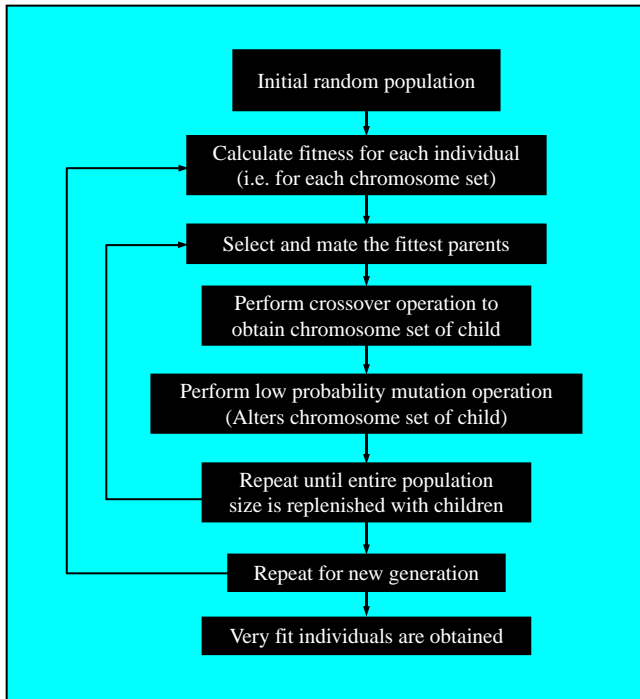


**Figure A1.**  
A genetic algorithm  
flow chart



15 0s and 1s. Binary representations of all the parameters of an individual (a point in the search space) are then attached to form a long string (i.e. a chromosome set).

- *Tournament selection.* Random pairs are selected from the population and the stronger individuals of each pair are allowed to mate and create a child. This process is continued until a new generation of size  $n$  is re-populated.
- *Single-point crossover.* Within this process, the chromosome set of the first (fitter) parent (e.g. 10101010) is mapped into that of the child. Then a crossover point is randomly chosen to the right of which the chromosome set of the second parent (e.g. 11001100) overwrites the chromosome of the first parent, for example. If the crossover point is exactly in the middle of the chromosome, the child's chromosome set for the case at hand is 10101100. The probability for single-point crossover  $P_{\text{cross}}$  is typically set to 0.6. This implies that the probability that the child would retain the entire chromosome set of the first parent is  $1.0 - P_{\text{cross}} = 0.4$ .
- *Uniform crossover.* In this case, the crossover can take place at any (and all) points of the parents' chromosome sets and the child can end up with any combination of its parents' chromosomes. The probability for uniform crossover is also typically set to 0.6. It should be noted that, in this case, it is quite unlikely that the child would inherit the entire chromosome set of either of its parents.
- *Jump mutation.* In this process, one or more child's chromosomes can mutate and the child can end up with a chromosome not present in either parent. Consequently, the jump mutation can cause one or more parameters to jump from one side of the range to the other. The probability of jump mutation is generally set equal to the inverse of the population size,  $P_{\text{mut}} = 1.0/n$ .
- *Creep mutation.* In this type of mutation, the value of one or more child's parameters is changed by a single increment but must remain within the prescribed range. The probability for creep mutation is also typically set equal to the inverse of the population size.
- *Elitism.* This operator is used to prevent a random loss of good chromosome strings during evolution. This is accomplished by ensuring that the chromosome set of the best individual generated to date is reproduced. If after the entire population of a new generation is generated through the processes of selection, crossover and mutation, the best individual is not replicated, then the chromosome set of the best individual is mapped into a randomly selected child in the new generation.

#### About the authors

M. Grujicic is a Professor in Materials Engineering in Clemson University. Grujicic's research interests include computational engineering. M. Grujicic is the corresponding author and can be contacted at: [mica.grujicic@ces.clemson.edu](mailto:mica.grujicic@ces.clemson.edu)

H. Marvi is a PhD Student in Clemson University. Marvi specializes in engineering dynamics.

G. Arakere is a PhD Student in Clemson University. Arakere's research interests include computational modeling.

I. Haque is a Professor in Mechanical and Automotive Engineering in Clemson University. He specializes in the area of vehicle dynamics.